AIAA SciTech Forum
23-27 January 2023, National Harbor, MD & Online
AIAA SCITECH 2023 Forum

10.2514/6.2023-0467

PIV Investigation of Turbulent Boundary Layer Response to Active Manipulation of Large-Scale Structures

Mitchell Lozier[1], Flint O. Thomas[2], Stanislav Gordeyev[3]
University of Notre Dame, Notre Dame, IN, 46556

It has been established that the dynamics of large-scale structures in the outer region of turbulent boundary layers and the dynamics of near-wall small-scale turbulence are correlated. In previous experiments using a single hot-wire; it was shown that synthetic large-scale structures introduced by a plasma-based actuator device in the outer region of the boundary layer had a strong modulating effect on the near-wall turbulence. The geometry of the actuator and the actuation frequency were optimized in previous experimental work to achieve the strongest modulation effect for the turbulent boundary layer of interest. In the study reported here, the optimized plasma-based actuator was placed into the outer region of a turbulent boundary layer and the response of the boundary layer to the synthetic large-scale structures was measured using planar particle imaging velocimetry. This measurement technique was used to measure the time-resolved two-dimensional velocity field downstream of the actuator over a large streamwise fetch. Detailed analysis of the particle imaging velocity data, including phase-locked measurements of the Reynolds stresses at each streamwise location were used to quantify the boundary layer response to the periodic spanwise-uniform actuation. The results and observations related to the mechanism of large-scale modulation of near wall small-scale turbulence are discussed.

I. Introduction

The large-scale structures (LSS) in the turbulent boundary layer (TBL) and their effect on technologically relevant flow properties such as skin friction drag, noise, and aero-optical distortion have been investigated extensively [1] [2] [3] [4] LSS refers in general to the coherent and energetic motions with a streamwise extent on the order of the boundary layer thickness that exist in high enough Reynolds number flows ($Re_\tau > 2000$) [1]. In the outer region of the TBL the LSS take the form of spanwise-oriented vortices whose coherent energy are concentrated around the geometric center of the log-linear region of the TBL ($y^+ = 3.9Re_\tau^{0.5}$) [1] [4]. Closer to the wall there is another coherent structure associated with streamwise vortices located in the buffer region that have a typical spanwise spacing on the order of the boundary layer thickness [1]. These streamwise vortical structures are responsible for the production of turbulence near the wall and have a significant effect on the global boundary layer dynamics as noted in many studies [2] [3].

In canonical boundary layers, thin shear layers, separating low-speed and high-speed regions (also called uniform momentum regions), have been observed and studied in the last few years [5] [6] These thin shear layer structures, combined with the low momentum flow underneath them,

---

[1] Graduate Student, Department of Aerospace and Mech. Eng., AIAA Student Member.
[2] Professor, Department of Aerospace and Mech. Eng., AIAA Associate Fellow
[3] Associate Professor, Department of Aerospace and Mech. Eng., AIAA Associate Fellow

are believed to be parts of a larger coherent structure, referred to as an Attached Eddy. A more recent investigation of adverse pressure gradient TBLs demonstrated that the local flow physics is largely dominated by an embedded shear layer associated with the inflectional instability of the outer mean velocity profile inflection point [7]. Using scaling laws developed for free shear-layers but applied to the adverse pressure gradient (APG) TBL, profiles of mean velocity and turbulence quantities exhibited a remarkable collapse. The generic applicability of the embedded shear layer scaling was demonstrated by collapsing multiple APG turbulent boundary layer data sets from the AFOSR-IFP-Stanford Conference compiled by Coles and Hirst [8]. Further support for the influence of the shear layer structure on the near-wall TBL dynamics was recently provided by a study demonstrating that the presence of a free shear layer just outside a TBL has a significant effect on the near-wall bursting/sweep events [9].

The ability to independently control outer layer LSS in the TBL offers new possibilities for studying their underlying dynamics. This aspect has remained largely unexplored and most studies or models regarding the relationship between the near wall small-scale and the outer large-scale structures deal with natural un-manipulated TBLs and apply various conditional-averaging techniques to study their interactions [2] [3]. Only a small number of studies have investigated modifying the LSS directly. In [3] an oscillating vertical plate was used to introduce a controlled traveling wave into the log-region of the boundary layer, and triadic interactions between the induced periodic structure and various scales in the boundary layer were studied. In [9] the turbulent boundary layer was externally forced by a shear layer and the turbulence inside the boundary layer was found to be both amplified and modulated by the external forcing.

Inspired by the results in [9], an active flow control device has been developed and used to introduce periodic large-scale disturbances into the outer region of the turbulent boundary layer using plasma-based forcing [10] [11] [12] [13] [14]. The boundary layer Reynolds number was kept low enough, so there is no energetic, naturally occurring, coherent large-scale structure present in the canonical flow. By introducing periodic motions as described above, a synthetic large-scale structure was introduced into the outer region of the boundary layer to mimic the naturally occurring coherent structures seen in higher Reynolds number flows. It was demonstrated previously that this active flow control device had sufficient authority within the boundary layer to produce a synthetic large-scale structure that could induce a measurable modulation effect on the near wall small-scale turbulent structures [13].

In this paper, we will use spatially and temporally resolved planar PIV to explore the development of the synthetic large-scale structures introduced by the actuator and their modulating effect on the small-scale structures near the wall. The results presented here highlight the analysis of boundary layer dynamics that can be performed using PIV. These results will also demonstrate that our PIV measurements are consistent with earlier hot-wire experiments as well as a spatial input-output model of the actuated TBL [13] [15].

II. Experimental Set-Up

As documented in previous experimental work [13], large-scale spanwise vorticity is introduced into the outer portion of the TBL using a novel active flow control device, called the Active Large-Scale Structure Actuator (ALSSA), seen in Figure 2(a). The ALSSA was configured to produce a pulsed, spanwise uniform, plasma-induced jet that serves to introduce coherent spanwise vorticity into the TBL at a specified frequency and user selected wall-normal location. To isolate the interactions of interest, the experimental studies were performed at $Re_\tau = 690$, which is low enough that there was no naturally occurring coherent large-scale structure in the outer portion of the canonical turbulent boundary layer. This approach allowed the controlled introduction of a synthetic, periodic, large-scale structure into the TBL. The fixed forcing frequency provides a well-defined reference frequency by which to phase-lock the measurements of the TBL response to obtain a clear and objective separation between the synthetic large-scale structure and the resulting changes to the TBL dynamics. One advantage of using this plasma-based method of actuation is that ALSSA introduces the synthetic structure at an experimentally selected height above the wall without physically altering the near-wall turbulence thru the presence of a wall mounted device.

The experiments presented here were performed in a low-turbulence, subsonic, in-draft wind tunnel located at the University of Notre Dame. To create the canonical turbulent boundary layer, a 2-meter-long by 0.6-meter-wide boundary layer development plate was installed along the center height of the tunnel test section. The main canonical turbulent boundary layer parameters are summarized in Table 1.

The ALSSA device, shown in Figure 2(a), is constructed on a rectangular plate of 2 mm thick (0.06δ) Ultem dielectric polymer. To create the spanwise uniform plasma jet, $0.05mm$ thick copper foil electrodes were installed on both sides of the actuator plate. Alternating current dielectric barrier discharge (AC-DBD) plasma was formed on the top side of the actuator using a high voltage AC source [16]. This source provided a 40kV peak-to-peak sinusoidal waveform excitation to the electrodes at a frequency of 4 kHz which provides a spanwise-uniform and steady plasma jet when active. The streamwise length of the actuator was chosen to be $L = 32\,mm$ ($< 1\,\delta$) to minimize the thin plate wake without creating arcing between the electrodes [13]. The spanwise length of the actuator plate was $W = 25\,cm$ ($8\,\delta$), which was determined to be sufficiently wide to ensure predominantly spanwise-uniform actuation [14]. The plasma electrodes were terminated $10mm$ from either end of the actuator plate. Symmetric airfoil-shaped vertical supports were used to position the actuator plate at a fixed wall-normal distance of $H/\delta = 0.3$ ($H^+ = 200$). The center of the plasma jet originates at a small distance above the plate [15] so the effective actuation height will be denoted as $H_p/\delta = 0.39$ $\left(H_p^+ = 265\right)$. This effective actuation height is demonstrated in Figure 1 where the physical plate and plasma jet locations are marked by vertical lines along with the streamwise mean velocity profile and turbulence intensity modified by the actuation. To introduce periodic forcing, the sinusoidal waveform described above was modulated by a square wave with 50 percent duty cycle at the experimental forcing frequency, $f_p = 80\,Hz$, ($f_p\delta/U_\infty = 0.4$). This forcing frequency was found to produce the largest turbulence modulation near the wall [13] and used for all subsequent experiments.

Table 1. Canonical turbulent boundary layer parameters at $x = 5\delta$

δ	U_∞	u_τ	C_f	H_{shape}	Re_θ	Re_τ
33.4 mm	6.95 m/s	0.31 m/s	0.0039	1.368	1770	690

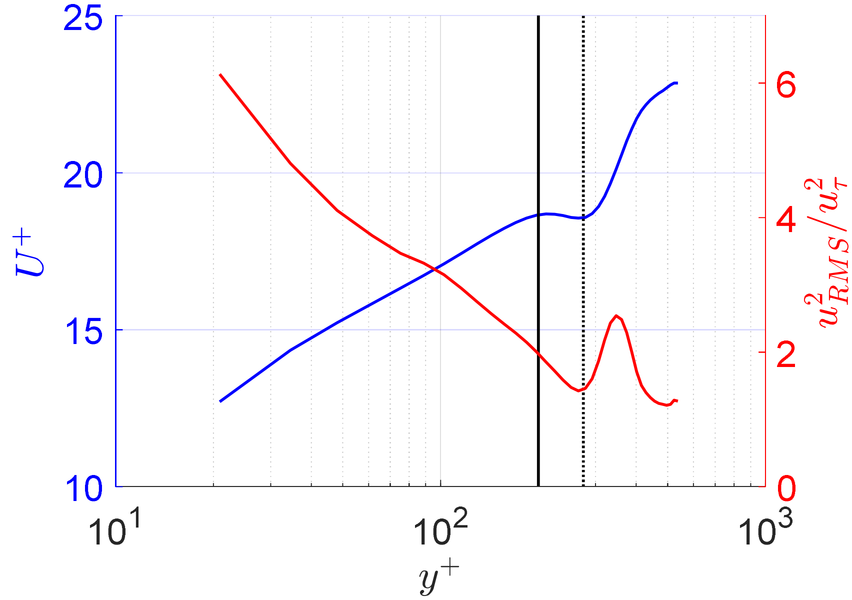

Figure 1. Profiles of streamwise mean velocity and turbulence intensity for actuated TBL downstream of ALSSA. Solid vertical line represents actuator plate location $H^+ = 200$. Dotted vertical line represents center of plasma jet $H_P^+ = 265$. $x = 1\delta, f_p = 80Hz$.

A schematic of the experimental set-up is shown in Figure 1(b). To measure the effect of the synthetic large-scale structure on the near-wall turbulence, a spatially and temporally resolved planar particle imaging velocimetry (PIV) system was used. To perform PIV measurements, the flow was seeded with DEHS particles (diameter <1μm) through the tunnel inlet and then illuminated with a dual pulsed 532 nm laser light sheet ($< 2mm$ spanwise thickness) directed through the top of the test section and down onto the boundary layer development plate. The laser sheet illuminated a measurement region of $x = 60mm \times y = 24mm$ ($x = 1.8\delta \times y = 0.7\delta$). Seven measurement regions were used with an overlap of 10 percent ($\Delta x_{ov} = 0.2\delta$) between neighboring regions resulting in a total experimental streamwise fetch of $x = 10\delta$. The closest measurement point to the actuator was limited to $x = 0.5\delta$ downstream of the trailing edge of the actuator due to physical constraints of the experimental setup. The separation between consecutive laser pulses was $\Delta t = 50\mu s$ resulting in a maximum expected particle displacement of $\Delta x_d^+ = 6$. Laser pulses were created with a repetition frequency of 12.5 Hz, phase-locked with the plasma forcing cycle. Images were captured with a Phantom v1840 high-speed camera at the lowest attainable sampling frequency of 100 Hz, again phase-locked with the laser pulses and plasma forcing cycle, and with the maximum exposure for each frame. The camera resolution was $1920 \times 1080\, px^2$. The resulting spatial resolution for the computed velocity vector fields was $\Delta x^+ = \Delta y^+ = 16$. The error of the computed velocity vectors was estimated to be $\varepsilon_u / U_\infty <$ 0.5% ($\varepsilon_u < 0.1u_\tau$). As mentioned above, the PIV image acquisition and plasma forcing cycles were phase locked, and due to the specific frequency chosen for the laser pulse repetition there were five distinct phases of the plasma forcing cycle measured. Over the total sampling time of

$T_s = 480\ sec$, each phase of the plasma forcing cycle was measured $n = 1{,}200$ times for convergence of the phase locked quantities (which will be introduced in the data reduction section). This PIV configuration resulted in measurements of the two-dimensional velocity field that were time- (or more specifically phase-) resolved, spatially resolved, and measured over a long streamwise extent downstream of the actuator.

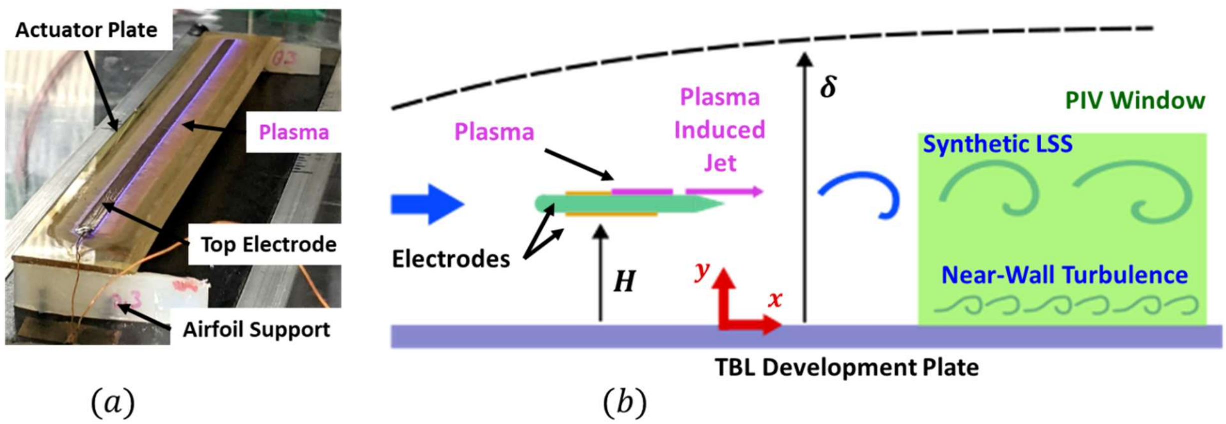

Figure 2. (a) photograph of plasma-based actuator device (ALSSA) and (b) schematic of experimental set-up.

III. Data Reduction

As discussed previously, since the actuator introduces periodic forcing into the flow, it is useful to phase-lock the PIV measurements to the plasma forcing cycle and perform a phase-locked analysis [9] of the results as described here. To start, a triple Reynolds decomposition of the velocity was considered, as shown in Equation 1,

$$u(x, y, t) = U(x, y) + \tilde{u}(x, y, \varphi) + u'(x, y, \varphi, n) \tag{1}$$

where u is the instantaneous velocity, U is the time mean component of velocity, $\tilde{u}$ is a phase dependent or modal velocity component, u' is a residual fluctuating component, φ is the phase, defined by the relationship in Equation 2, where n is the number of realizations as described below.

$$t_n = \left(\frac{\varphi}{2\pi} + n\right) T_p \tag{2}$$

Here t_n is a time in the n^{th} realization, which is related to the phase angle, φ, by the period of the plasma forcing cycle, $T_p = 1/f_p$. To ensure this relationship was maintained the plasma forcing and PIV acquisition were synchronized as described in the experimental setup. These n realizations were then ensemble averaged to compute the modal component of velocity as a function of the phase angle, $\tilde{u}(x, y, \varphi)$. This same process can be repeated for other quantities of interest in order to measure how they change with phase. This process will be denoted by the tilde operator, similar to the streamwise modal velocity above, in the subsequent analysis.

The remaining fluctuating component of the velocity, u' was then used to compute a new quantity referred to as the residual turbulence. The residual turbulence is an ensemble-averaged

RMS of the residual fluctuating component of velocity as shown in Equation 3. More specifically the changes in the residual turbulence $\Delta u'_{rms}$ as computer in Equation 4 will be presented and discussed in detail in the experimental results.

$$u'_{rms}(x, y, \varphi) = (\langle [u'(x, y, \varphi, n)]^2 \rangle_n)^{\frac{1}{2}} \tag{3}$$

$$\Delta u'_{rms}(x, y, \varphi) = u'_{rms}(x, y, \varphi) - \langle u'_{rms}(x, y, \varphi) \rangle_{\varphi} \tag{4}$$

IV. Results

The effect of the ALSSA device on the baseline canonical boundary layer has been quantified in previous experimental work and discussed in earlier papers [12] [13] [14]. The results presented here will be focused on new analysis that has been made possible by taking PIV measurements, and observations about these new results that provide insight into the mechanism of near wall turbulence modulation by the imposed synthetic large-scale structures. To begin, a spatially resolved map of the streamwise component of modal velocity obtained via PIV is presented in Figure 3(a) for a single phase. Here the physical location of the actuator is shown by the thin red rectangle on the left-hand side of the figure. Above the actuator there are strong periodic fluctuations in the streamwise modal velocity associated with the synthetic large-scale structures being produced by the actuator. There are also strong fluctuations in the region between the actuator and the wall, with the highest amplitude primarily in the log-region, that occur slightly downstream of the fluctuations above the actuator. The induced variations in the streamwise modal velocity below the actuator also extend down nearly to the wall though the amplitude of the variations begins to diminish approaching the wall.

Figure 3(b),(c) are maps of the streamwise component of modal velocity obtained from hot-wire experiments [13] and a spatial input-output model of the actuated boundary layer [15] respectively. Since the hot-wire provides data only at a single streamwise point, the hot-wire data has been pseudo-spatially reconstructed in the streamwise direction from the phase of multiple single-point measurements [13]. It shows that when properly reconstructed there is good agreement with the PIV results in both phase and amplitude, especially in the log-region of the boundary layer between the actuator and the wall. Similarly, the results from the spatial input output model also have a good agreement in amplitude and phase with the PIV results in the region below the actuator. In comparison to the PIV results, it can be observed that the spatial input-output results do not account for diffusion effects and the fluctuations in streamwise modal velocity remain mostly confined to a single wall-normal region whereas the experimental results tend to blend, and distinct wall-normal regions become less apparent downstream. The comparison of the results from these three experiments serves as a partial validation of the current PIV measurements as well as a reminder of the previous work already done to quantify the effect of ALSSA on the canonical TBL.

Using the measurements of the streamwise modal velocity presented in Figure 3, the phase-speed of fluctuations which are phase-locked with the plasma forcing were estimated as follows: using the hot-wire data from previous experiments [14], the phase-speed at each wall-normal position was estimated by tracking the time, which is related to phase in Equation 2, at which a maximum or minimum in the modal velocity signal arrived at each streamwise measurement station. The average phase-speed over a specific region can be found by dividing the streamwise separation between two measurement locations by the difference in computed arrival times. More information about the details of the algorithm can be found in [13]. The resulting estimates of the phase-speeds are presented in Figure 4 as black squares.

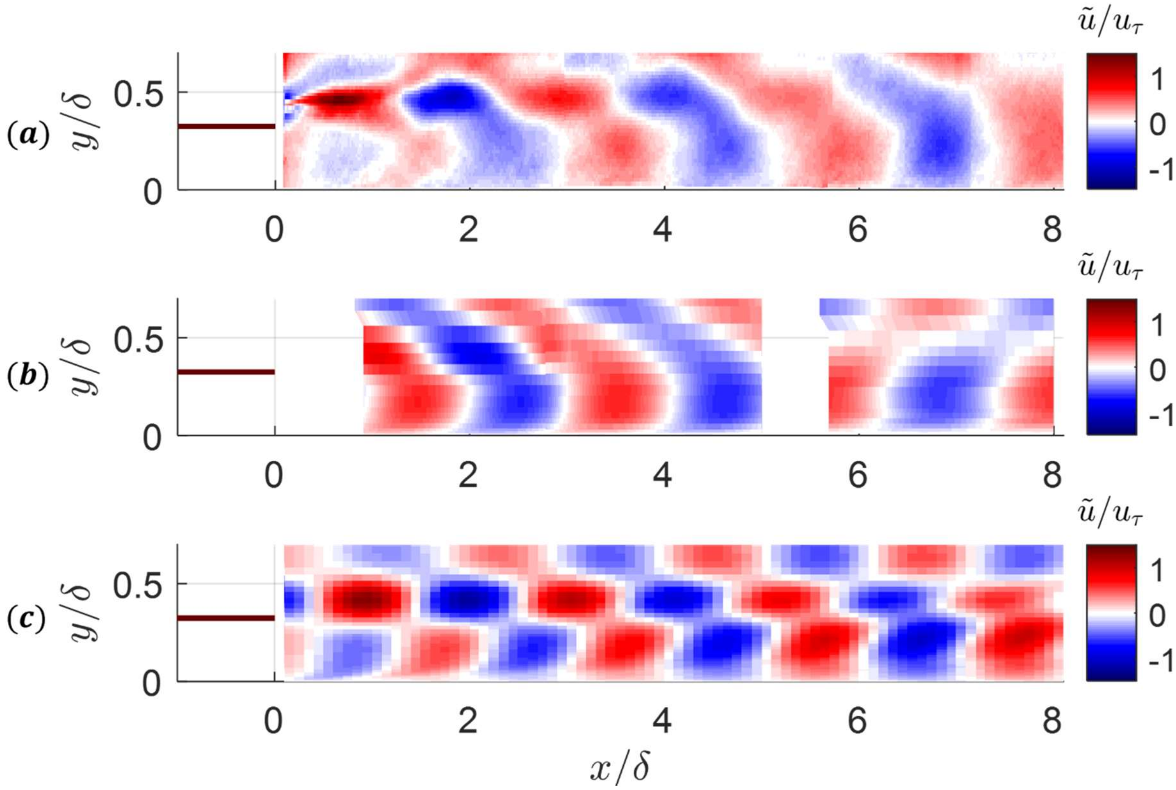

Figure 3. Streamwise component of modal velocity from (a) PIV (b) hot-wire [13] (c) spatial input-output model [15] $H^+ = 200, f_p = 80Hz$.

In the case of the new spatially resolved PIV data, the phase-speed was estimated by computing the spatial cross-correlation of pairs of modal velocity signals, at specified wall-normal locations with sequential phases (for example, $\tilde{u}(y, x, \varphi = 0)$ and $\tilde{u}(y, x, \varphi = 2\pi/5)$). The individual cross-correlations were averaged over all 5 pairs of sequential phases to improve the estimate of the phase-speed at each location. The streamwise locations of the positive and negative peaks in the spatial cross-correlation and the period of the plasma forcing cycle were then used to determine the average phase-speed over each measurement region, shown in Equation 5, and results are shown in in Figure 4 as blue circles.

$$u_{\varphi_{PIV}}(x, y) = \frac{\Delta x(R_{max}) - \Delta x(R_{min})}{0.5T_P} \tag{5}$$

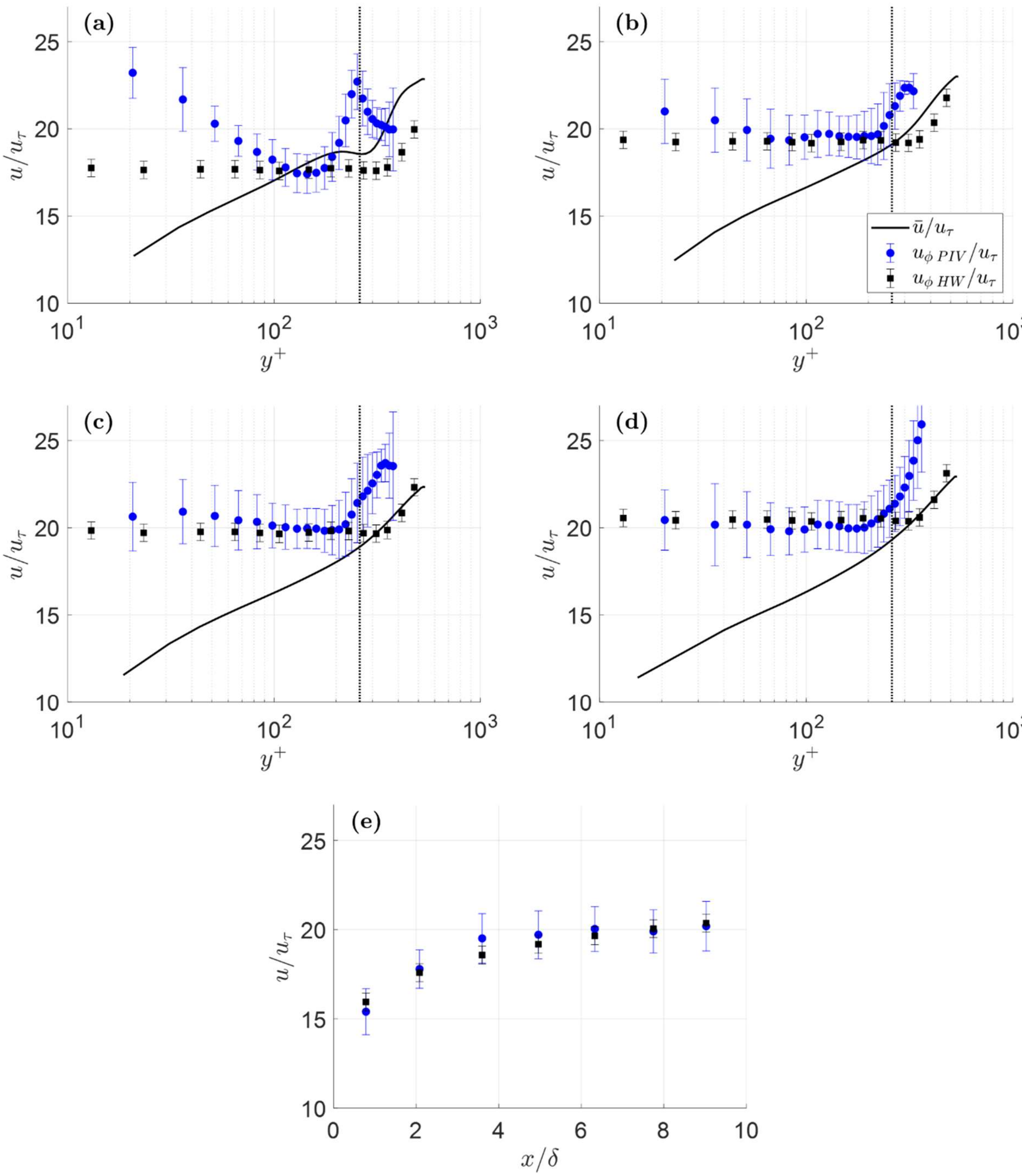

Figure 4. Profiles of mean velocity (solid black line) and phase-speed measured using hot-wire (black squares) or PIV (blue circles), with 90% confidence interval. Streamwise locations of (a) $x = 2\delta$, (b) $x = 5\delta$, (c) $x = 6.5\delta$, (d) $x = 9\delta$. (e) Streamwise development of phase-speed measured at $y^+ = 100$. $H_P^+ = 265, f_p = 80Hz$.

There is a good agreement in the estimated phase-speed between the hot-wire and PIV methods across all streamwise locations after $x = 5\delta$, especially within the log-region of the boundary layer as demonstrated in Figure 4(e). The observed similarities between the spatially resolved PIV results and the spatially reconstructed hot-wire measurements in Figure 3 demonstrate the accuracy of the methods used to estimate phase-speed. In Figure 4, above the actuator height the phase-speed of phase-locked fluctuations appear to be converging with the local mean velocity especially at the farthest downstream locations Figure 4(c),(d). Below the actuator height the phase-speed appears to be nearly constant with a magnitude that is similar to the mean velocity at the location of the plasma jet. This observation suggests that the phase-speed of fluctuations below the actuator are strongly correlated with the speed of the synthetic large-scale structures produced by the actuator. In Figure 4(e) the phase-speed within the log-region appears to be reaching an asymptote at the farthest downstream locations. This phase-speed asymptote may be important in characterizing how the boundary layer adjusts to the presence of synthetic large-scale structures.

Additional phase-locked quantities will next be presented to characterize the turbulence modulation effect of the synthetic LSS produced by the actuator and make observations about the dynamics of LSS within the TBL. A map of the changes in residual turbulence is presented in Figure 5(a). Similar to the streamwise component of modal velocity discussed above, the amplitude and spatial distribution of the residual turbulence seen in the PIV results here is consistent with earlier measurements of the residual turbulence made using hot-wires [13].

The map of residual turbulence can be easily divided visually into two distinct regions, above and below the actuator. Above the actuator there are strong fluctuations in the residual turbulence which were shown to be a signature of the synthetic LSS convecting downstream from the actuator [13]. These fluctuations are strongest immediately downstream of the actuator and tend to decay in amplitude as they convect downstream. In the region below the actuator, which is the log-region of the boundary layer, there are also strong fluctuations in the residual turbulence which are characteristic of the modulation of small-scale turbulence by the synthetic LSS. These fluctuations in residual turbulence, or regions of modulated turbulence, are the focus of the current experiments and analysis. The positive fluctuations in modulated turbulence occur slightly downstream of positive peaks in the streamwise modal velocity. It can be seen that these fluctuations initially grow in amplitude reaching a maximum at a downstream location of approximately $x = 6\delta$ and a wall-normal distance near the geometric center of the log-region, $y^+ = 100$. The streamwise location of the maximum turbulence modulation corresponds to an effective convective timescale of $T^+ = 300$ (or $TU_\infty/\delta = 10$). In earlier experimental work it was found that the mean velocity profile of the actuated wake produced by ALSSA could be extracted and the wake was found to have nearly canonical growth despite being embedded within the TBL [12]. Using these previous measurements of the actuated wake development it is expected that the portion of the actuated wake below the actuator will intersect the wall around the streamwise region where the amplitude of the modulation of the residual turbulence reaches its maximum. This observation suggests that the physical interaction of the actuated wake with smaller scale turbulent structures near the wall may have an impact of the development or the strength of the modulation effect.

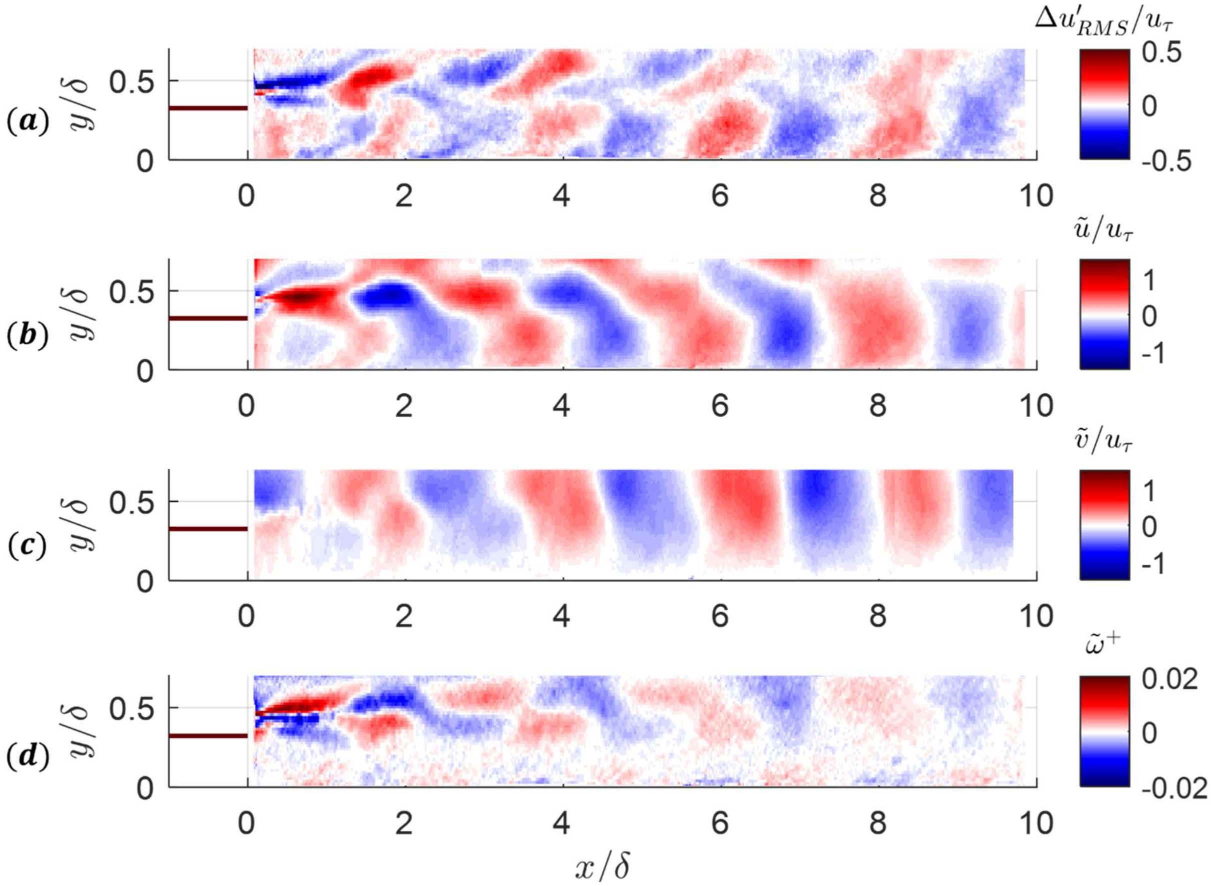

Figure 5. Map of the (a) changes in residual turbulence (b) streamwise component of modal velocity (c) wall normal component of modal velocity (d) modal fluctuations in spanwise vorticity. $H^+ = 200, f_p = 80Hz$.

In Figure 5(b),(c) the streamwise and wall-normal components of the modal velocity respectively are presented. Similar to the observations made about the streamwise modal velocity earlier, the variations in wall-normal modal velocity are relatively strong and periodic at and above the actuator height. In the region below the actuator and through the log-region there are relatively weaker variations in the wall-normal modal velocity that exist but these fluctuations decay closer to the wall which is expected given the solid boundary. In the log-region the positive variations in wall-normal modal velocity appear to be slightly ahead of the positive variations in streamwise modal velocity. It is noteworthy that the measurements of streamwise and wall-normal modal velocity in this experiment, presented in Figure 5, are similar in both amplitude and spatial distribution to the same quantities measured in experiments where large-scale motions were introduced via dynamic wall roughness [17]. This similarity in results demonstrates again that the actuator design used here can achieve effective large-scale modification of the log-region and near-wall regions without being physically located in the near wall region.

In Figure 5(d) a map of the phase-locked variation in the spanwise vorticity is presented. Here the spanwise vorticity (assumed positive for counter-clockwise rotation) is defined in Equation 6 and the computed measurements of vorticity have been normalized by the appropriate inner-scales,

$$\widetilde{\omega} = \frac{d\tilde{v}}{dx} - \frac{d\tilde{u}}{dy} \tag{6}$$

There are regions of strong positive and negative spanwise vorticity at and above the actuator location associated with the synthetic LSS being produced by the actuator. These concentrated spanwise vorticity variations immediately downstream of the actuator become a single, more diffuse, but still periodic region as the synthetic LSS convect downstream. In the log-region below the actuator and much closer to the wall, there appear to be additional variations in the spanwise vorticity which are in a region that is spatially distinct or separated from the variations directly associated with the synthetic LSS. This near wall spanwise vorticity is well aligned in the streamwise coordinate with the LSS spanwise vorticity above the actuator but has the opposite sign, most easily visualized further downstream. These near wall variations in spanwise vorticity appear to be opposite in phase with changes in residual turbulence and streamwise modal velocity near the wall. The presence of this near wall spanwise vorticity may be related to the mechanism of turbulence modulation near the wall. Further investigation to determine the role of this spanwise vorticity and how it is being generated may be important in understanding the dynamics of LSS within the TBL.

The streamwise modal velocity is re-plotted in Figure 6(a) where the y-scale has been converted to inner units and the scale is logarithmic in order to better visualize the region below the actuator and more specifically the log-region. The minimum wall-normal distance shown in the maps in Figure 6 is $y^+ = 30$. The map of residual turbulence downstream of the actuator is also re-plotted in Figure 6(b). It is now clearer how the maximum amplitude of the turbulence modulation is developing as the synthetic LSS convect downstream. The inclination of these regions of modulated turbulence can also be more easily seen where the higher amplitude modulation occurs near the geometric center of the log-region ($y^+ = 100$) and occurs farther downstream than the related fluctuation closer to the wall. In previous experiments it was determined that the inclination of the modulated turbulence was closely related to the canonical inclination of attached eddies [6]. It can also be seen now that for a single pairing of negative and positive fluctuations in the residual turbulence ($x = 6 - 7\delta$), the transition from negative to positive amplitude upstream occurs over a shorter streamwise distance than the opposite transition from a positive to negative amplitude. This suggests that the process of turbulence modulation is not linear, otherwise the fluctuations in residual turbulence would follow a more evenly periodic shape like that seen in the streamwise modal velocity. This was also seen in previous experiments where a quasi-steady analysis showed the relationship between streamwise modal velocity and residual turbulence was not linear immediately downstream of the actuator but was becoming more linear as the TBL responded and adjusted to the synthetic LSS further downstream [12]. With an expanded view of the log-region it is now easier to see that positive changes in the residual turbulence occur in phase with a positive to negative streamwise change in the modal velocity.

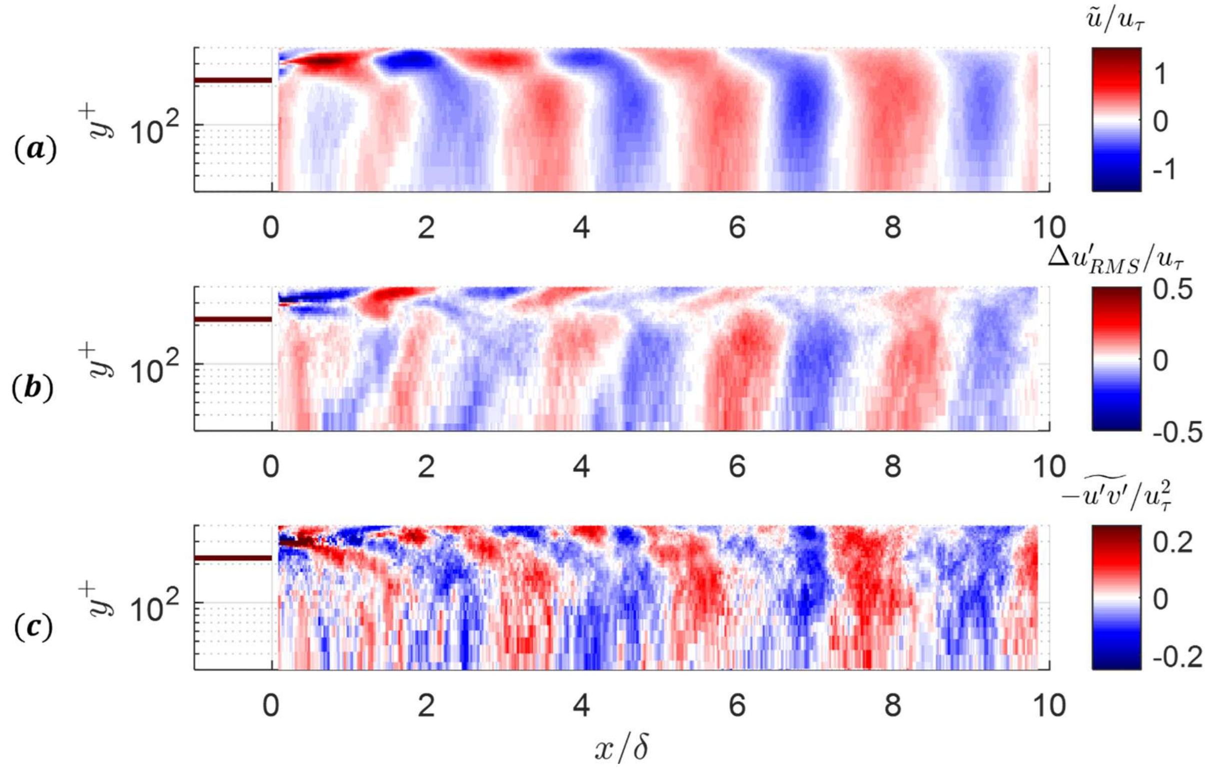

Figure 6. (a) streamwise component of modal velocity (b) change in residual turbulence (c) modal fluctuations in Reynolds stress. $H^+ = 200, f_p = 80Hz$.

Phase-locked variations in the Reynolds stress, another quantity specifically targeted using PIV, have been plotted in Figure 6(c). Here the instantaneous measurements have been computed and phase averaged like the streamwise modal velocity (as described in the data reduction section). The strongest changes in the Reynolds stress are again concentrated within the log-region and have a similar asymmetrical periodicity as the residual turbulence. In this case the variations in the Reynolds stress appear to occur slightly upstream of the changes in the residual turbulence, or it could be said that peak Reynolds stress lags peak residual turbulence. Changes in the Reynolds stress and a changing mean streamwise velocity gradient due to the modal velocity could be indications of a change in the local turbulence production within the log-region. Further investigation of the changes in Reynolds stress may be important in understanding how the large-scale structures in the outer region modulate the turbulence near the wall.

V. Conclusions

PIV experiments were conducted to measure the two dimensional, spatially resolved and phase resolved, velocity field downstream of the ALSSA actuator. The results of these experiments were consistent with earlier experimental work involving hot-wire measurements as well as a spatial input-output model of the actuated boundary layer. The results also showed an encouraging similarity to experiments conducted using dynamic wall roughness confirming the effectiveness of the current actuator which is not limited to the near wall region.

Turbulence modulation, in the log-region specifically, was observed as an effect of the synthetic large-scale structures produced by the actuator. The comparison between the regions of modulated turbulence and the large-scale streamwise and wall-normal motions produced by the actuator showed that the response of the TBL was nonlinear and not immediate as the maximum amplitude of turbulence modulation occurred a significant distance downstream of the actuator trailing edge.

Leveraging the benefits of making planar PIV measurements, the variations in spanwise vorticity and Reynolds stress within the actuated boundary layer were also presented and analysed for the first time. Significant variations in both quantities occur within the log-region, and are separated spatially from the synthetic LSS, which suggest different mechanisms by which the synthetic LSS might have a modulating effect on the turbulence near the wall.

Further analysis of the PIV results presented here is ongoing to determine the mechanism by which the outer LSS modulate the small-scale turbulence within the log-region and what this reveals about the dynamics of natural coherent LSS within canonical TBLs.

VI. References

[1] N. Hutchins and I. Marusic, "Large-scale influences in near-wall turbulence," *Phil. Trans. R. Soc. A,* vol. 365, pp. 647-664, 2007.

[2] S. Duvuuri and B. McKeon, "Phase relations in a forced turbulent boundary layer: implications for modelling in high Reynolds number wall turbulence," *Phil. Trans. A,* vol. 375, 2017.

[3] S. Duvuuri and B. McKeon, "Triadic scale interactions in a turbulent boundary layer," *J. Fluid Mech.,* vol. 767, p. R4, 2015.

[4] S. K. Robinson, "Coherent Motions in the Turbulent Boundary Layer," *Ann. Rev. Fluid Mech.,* vol. 23, pp. 601-639, 1991.

[5] C. M. de Silva, N. Hutchins and I. Marusic, "Uniform momentum zones in turbulent boundary layers," *J. Fluid Mech.,* vol. 786, pp. 309-331, 2016.

[6] R. J. Adrian, C. D. Meinhart and C. D. Tomkins, "Vortex organization in the outer region of the turbulent boundary layer," *J. Fluid Mech.,* vol. 422, pp. 1-53, 2000.

[7] D. M. Schatzman and F. O. Thomas, "An experimental investigation of an unstready adverse pressure gradient turbulent boundary layer: embedded shear layer scaling," *J. Fluid Mech.,* vol. 815, pp. 592-642, 2017.

[8] D. E. Coles and E. A. Hirst, "Comutation of Turbulent Boundary Layers: Compiled Data," in *AFOSR-IFP*, Stanford University, 1968.

[9] P. Ranade, S. Duvuuri, B. McKeon, S. Gordeyev, K. Christensen and E. J. Jumper, "Turbulence Amplitude Amplification in an Externally Forced, Subsonic Turbulent Boundary Layer," *AIAA Journal,* vol. 57, pp. 3838-3850, 2019.

[10] M. Lozier, S. Midya, F. Thomas and S. Gordeyev, "Experimental Studies of Boundary Layer Dynamics Using Active Flow Control of Large-Scale Structures," in *TSPF-11*, Southhampton, UK, 2019.

[11] M. Lozier, F. O. Thomas and S. Goredyev, "Experimental Studies of Boundary Layer Dynamics via Active Manipulation of Large-Scale Structures," in *TSFP-12*, Osaka Japan, 2022.

[12] M. Lozier, F. Thomas and S. Gordeyev, "Streamwise Evolution of Turbulent Boundary Layer Response to Active Control Actuator," in *AIAA Scitech*, 2020.

[13] M. Lozier, F. O. Thomas and S. Gordeyev, "Turbulent Boundary Layer Repsosne to Active Control Plasma Actuator," in *AIAA Scitech*, 2021.

[14] M. Lozier, F. O. Thomas and S. Gordeyev, "PIV Investigation of the Turbulent Boundary Layer Response to Active Control Actuator," in *AIAA Scitech*, 2022.

[15] C. Liu, I. Gluzman, M. Lozier, F. Thomas, S. Gordeyev and D. Gayme, "Spatial input–output analysis of large-scale structures in actuated turbulent boundary layers," *AIAA Journal,* vol. 60, pp. 6313-6327, 20222.

[16] F. O. Thomas, T. C. Corke, M. Iqbal, A. Kozlov and D. Shatzman, "Optimization of SDBD Plasma Actuators for Active Aerodynamic Flow Control," *AIAA Journal,* vol. 47, pp. 2169-2178, 2009.

[17] D. Huynh and B. McKeon, "Characterization of the Spatio-Temporal Repsonse of a Turbulent Boundary Layer to Dynamic Roughness," *Flow, Turbulence and Combustion,* vol. 104, pp. 293-316, 2019.

[18] M. Wicks and F. O. Thomas, "Effect of Relative Humidity on Dielectic Barrier Discharge Plasma Actuator Body Force," *AIAA Journal,* vol. 53, 2015.

[19] R. Mathis, N. Hutchins and I. Marusic, "Large-Scale Amplitude Modulation of the Small-Scale Sturcutres in Turbulent Boundary Layers," *J. Fluid Mech.,* vol. 658, pp. 311-336, 2009.